Journal of Mines, Metals and Fuels, *73(1): 37-48; 2025. DOI: 10.18311/jmmf/2025/45238*

Print ISSN : 0022-2755

Journal of Mines, Metals and Fuels

Contents available at: *www.informaticsjournals.co.in/index.php/jmmf*

Protection from Noise in Control Rooms of Ore Handling and Mineral Beneficiation Plants Using Acoustic Metamaterials

Nihar Ranjan Sahu[1] and Bibhuti Bhusan Mandal[2]*

[1]Noise Lab, Department of Mining Engineering, Indian Institute of Technology, Kharagpur – 721302, West Bengal, India;

[2]Department of Mining Engineering, Indian Institute of Technology, Kharagpur – 721302, West Bengal, India; bbmandal@gmail.com

Abstract

Acoustic Metamaterials (AMMs) are emerging as potential solutions for soundproofing and acoustic insulation challenges. In India 12.4 to 25.7% of mining employees suffer Noise-Induced Hearing Loss (NIHL) due to the high noise level. Noise levels in ore beneficiation plants exceed permissible limits, frequently reaching 115 dB(A) or greater. This study focuses on designing configurable AMM for constructing control rooms in ore handling and mineral beneficiation plants, aiming for a minimum attenuation of 15dB within the critical 3-6 kHz range. Here, a novel method employing Simple Expansion Chamber (SEC) frames to achieve customisable acoustic insulation characteristics within AMM has been introduced. Utilising 3D printing technology, five samples of 10mm thickness and 29.8mm ϕ were fabricated using photopolymer resin, each featuring an internal SEC structure with inlet and outlet ports. The diameter of SEC for all five samples varies from 2mm to 4.47mm which causes the variation of area expansion ratio from 4 to 20, keeping the length of SEC constant. The Sound Transmission Loss (STL) is measured across 1-6kHz frequencies using an Impedance Tube Apparatus (ITA).

***Major Findings:** Our findings indicate that the STL of all five samples ranges from 11.8dB to 46dB between 1 and 2.7kHz and above 2.7kHz from 20dB to 32.4dB with a periodic trend. For all five samples, the STL is at least 21.5dB in the specially targeted frequency range of 3-6kHz. These results highlight how the diameter of SEC affects the acoustic insulation characteristics of the metamaterial. The proposed material offers promising applications in the construction of ventilated and soundproof control rooms for the protection of operators from noise-induced hearing loss.*

Keywords: *Acoustic Metamaterial, Noise-Induced Hearing Loss, Protection From Hearing Loss, Simple Expansion Chamber, Soundproof Control Rooms*

1.0 Introduction

Following the excavation of minerals from mines, further processing takes place through Ore Handling Plants (OHP) and mineral beneficiation facilities. Both OHP and beneficiation plants comprise high-power crushers, mills, vibrating screens and hydrocyclones all of which are traditionally infamous for being noisy. Exposure to noise at the workplace is a well-known occupational hazard. Occupational noise is responsible for 16% of adult hearing loss that is incapacitating worldwide, with sub-regional differences ranging from 7 to 21%[1]. Studies on health surveillance in India have shown that 12.4 to 25.7% of mining employees suffer from NIHL[2]. The NIHL commonly occurs in 3-6 kHz region with a threshold of 4 kHz[3,4]. Studies across many countries have repeatedly indicated that noise levels in ore beneficiation plants often exceed permissible levels, frequently reaching

*Author for correspondence

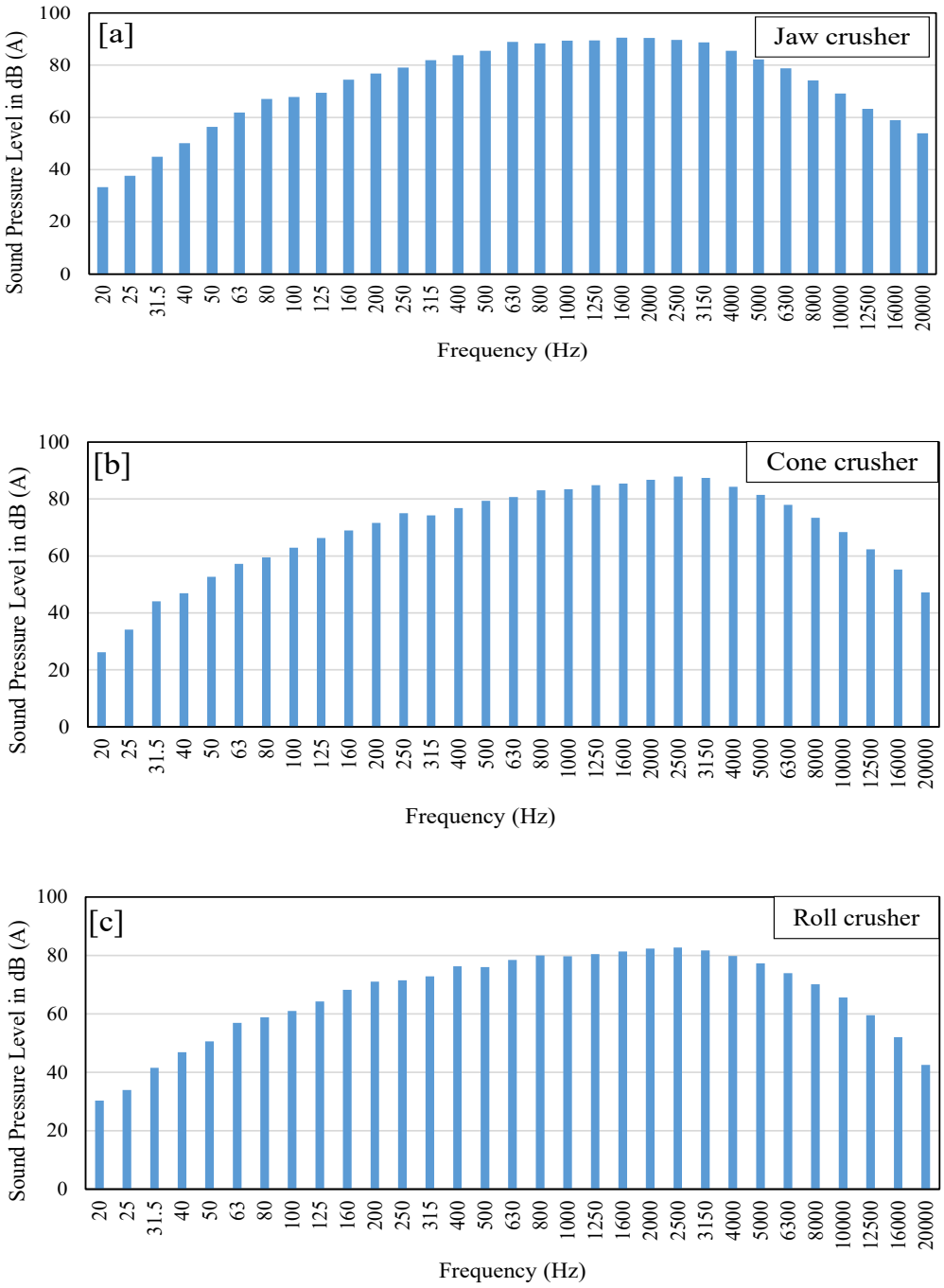


Figure 1. 1/3 Octave band frequency vs SPL in A- weighting scale measured near **(A)** Jaw crusher; **(B)** Cone crusher; **(C)** Roll crusher.

115dB(A) or greater[5,6]. The authors recently performed a noise inspection in a mineral beneficiation plant within the leasehold area of an open pit iron-ore mine in central India. Equivalent continuous sound pressure levels (L_{eq}) measured by a sound level meter close to the operators' position exceeded 100dB(A) at most of the places. These noise levels remained nearly steady throughout the measurement, which is typical of highly mechanised processing facilities. The frequency distribution of the recorded noise in the 1/3rd octave band has been depicted in Figure 1.

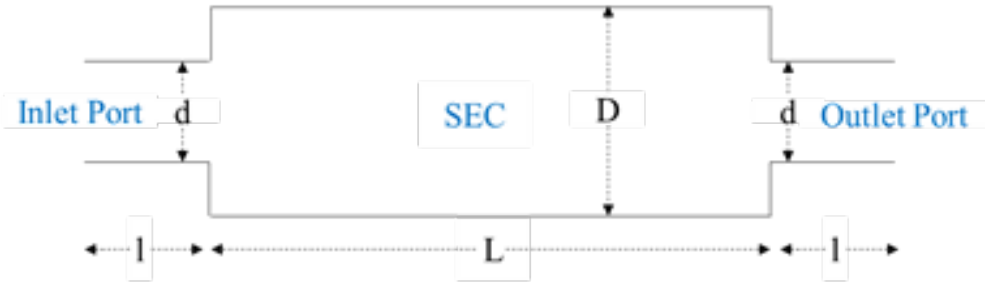


Figure 2. Structure of a simple expansion chamber.

The anticipated harmful effects of noise exposure in the processing plants prompted the present authors to "design and construct" a suitable control room made of a specific AMM, which would be capable of rendering sufficient hearing protection to the operators. The AMM would attenuate noise by about 15dB in the 3-6kHz region which is more vulnerable to occupational hearing loss[7]. Thus the noise exposure of the affected personnel would be brought within the legal limits set by the Directorate General of Mines Safety (DGMS)[8] through a protective enclosure. Nevertheless, an appropriate AMM capable of reducing the surrounding noise by at least 15dB during transmission must be developed.

The authors first looked at using an SEC structure because of their exceptional acoustic qualities. Since the SEC structures can reduce noise and enhance acoustic performance, they are frequently used in a variety of acoustic applications including mufflers, resonators and silencers (Figure 2). Periodic Sound Transmission Loss (STL) was reported to occur throughout a broad frequency range in *SEC* structures[9-11]. Using 3D printing, one can explore SEC structures of a few millimetre dimensions that were previously not feasible with conventional production techniques, with the help of the design freedom and flexibility it offers.

The acoustic insulation property of 3D printed AMM with varying area expansion ratio (m) of SEC structure has not been explored so far. Therefore, the focus of the present research is to investigate the impact of the area expansion ratio of *SEC* structure on acoustic insulation characteristics and the application potential of the metamaterial in the design of the control rooms for ore handling and mineral beneficiation plants.

2. Materials and Methods

2.1 Materials Used for 3D Printing of Samples

The samples are 3D printed from photopolymer resin (manufacturer: WOL 3D). The material properties of the photopolymer resin indicate its promising application as a building material[12,13].

2.2 Unit Cell Design

For the design of samples, unit cells are typically constructed as the starting point for developing into a periodic assembly. Based on this unit cell design approach, a variety of materials have been created and produced by many researchers for acoustic and mechanical applications, including those with hexagonal-shaped Helmholtz resonators[14], inline cavity [12,15], perforated hemispherical shell[16], membrane resonator[17], octet truss[18-21], isotropic truss[18], body-centred cubic[22], face diagonal cubic[22], octahedron[22,23], void octet[22], open cell foam[24,25], kelvin foam[21,26] and truncated octahedron[22]. In the present research work authors have considered a SEC as an internal structure due to exceptional acoustic qualities. The prior research[11,27,28], for the design of AMM with internal SEC structure shows greater acoustic absorption and insulation characteristics for inlet and outlet port lengths of 1mm. Since these elements substantially impact acoustic absorption and acoustic insulation characteristics, the present authors have considered all the above parameters for the design of the unit cell.

$$Area\ expansion\ ratio\ (m) = \frac{cross\ sectional\ area\ of\ SEC}{cross\ sectional\ area\ of\ inlet\ port}$$

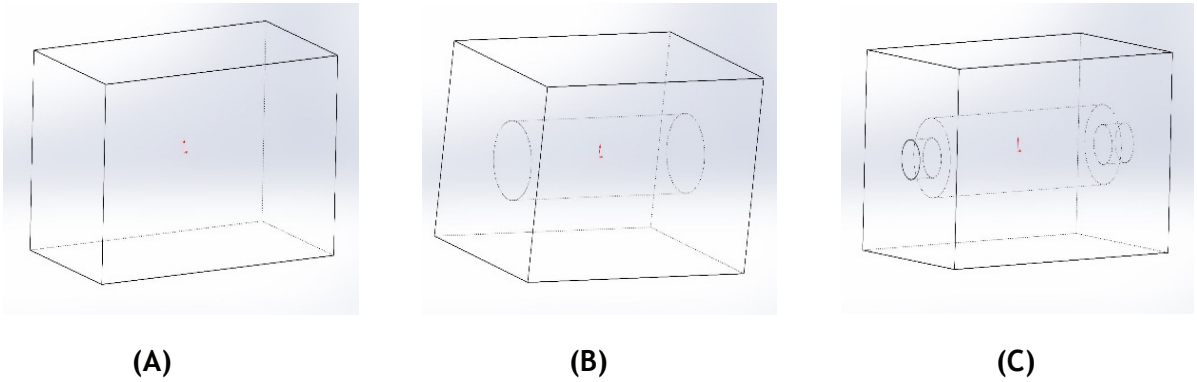


Figure 3. Steps of unit cell design.

For the preparation of samples, a Stereolithography 3D printer with a working resolution of roughly 1mm was used. Therefore, cylindrical ports with a diameter and a length of 1mm were used for the best possible printing with the available facility. To get m= 4, a cylindrical SEC of 2mm ϕ is chosen and the length of SEC is selected as 8mm for perfect printing. After investigating the length of SEC and two 1mm-long ports on either side, the ideal size of the unit cell is found to be 5 × 5 × 10mm. It is noteworthy that expanding the unit cell past this point will unavoidably result in a reduction of the sample's perforation ratio.

Unit cells were designed in SOLIDWORKS software. The procedure starts with creating a solid cubic unit cell and then extracting the cylinders from it. Because of this extraction, an internal SEC with respective outlet and inlet ports is created. A quick description of the unit cell design procedure is given below:

Step 1: A 5×5×10mm solid cuboid unit cell is created using SOLIDWORKS' extrude feature (Figure 3(A)).

Step 2: From the centre of the unit cell, an 8mm long and 2mm ϕ cylinder is removed using the cut extrude facility (Figure 3(B)).

Step 3: Cylinder with 1mm ϕ and 10mm length is removed through the centre of the SEC. The procedure results in the design of unit cell-1 with an *SEC* of length 8mm attached to the inlet and outlet ports (Figure 3(C)). Similarly, other unit cells (from 2 to 5) are created by varying the diameter of SEC 2.83mm, 3.46mm, 4mm and 4.46mm.

2.3 How the Samples are Designed

To fabricate a sample with specific dimensions, the process begins with the design of a seed or unit cell in SOLIDWORKS and thereafter generates a periodic multitude of these cells to create the samples with realistic dimensions. The Impedance Tube Apparatus (Model: HO-AE-ITA-219) recommends cylindrical samples of 29mm ϕ for determination of acoustic insulation characteristics of AMM in the 1-6 kHz frequency range[29].

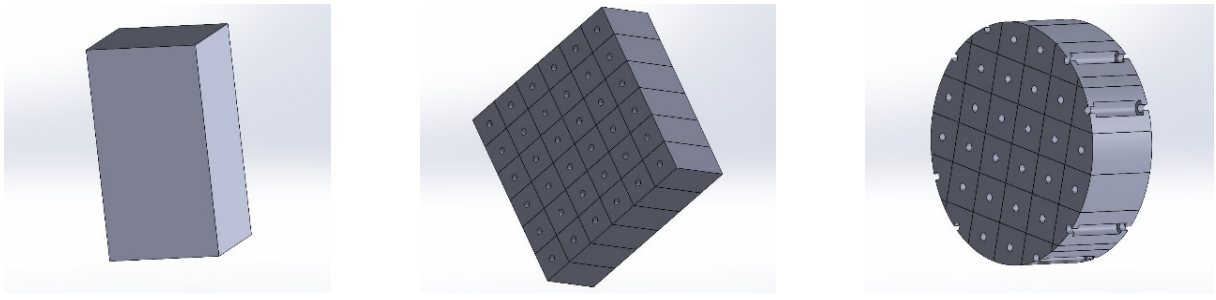


Figure 4. Procedure for designing samples.

Table 1. Sample specifications

Sample Id	Parameters						
	Diameter of sample (ϕ) (mm)	Thickness of sample (mm)	Diameter of SEC (D) (mm)	Length of SEC (L) (mm)	Diameter of inlet and outlet ports (d) (mm)	Length of inlet and outlet ports (l) (mm)	Area expansion ratio (m)
M1	29.8	10	2.00	8	1	1	4
M2	29.8	10	2.83	8	1	1	8
M3	29.8	10	3.46	8	1	1	12
M4	29.8	10	4.00	8	1	1	16
M5	29.8	10	4.47	8	1	1	20

In practice, the samples are fixed at 29.8mm ϕ to perfectly match the inner diameter of the measurement tube. Unit cell-1 is imported into SOLIDWORKS for the design of sample M1 (29.8mm ϕ and 10mm thickness), as shown in Step 1 (Figure 4). Then, as Step 2 (Figure 4) illustrates, six periodic designs of the unit cell are made along the x and y-axis, forming a rectangular cuboid of 30mm × 30mm × 10mm. The cuboid is then cut, as shown in Step 3 (Figure 4), to create a cylindrical sample with 29.8mm ϕ and 10mm thickness. Similar to this, unit cells 2, 3, 4 and 5 are used to create the other samples. Table 1 provides the specifications of each sample.

2.4 Fabrication of Samples

Out of all the 3D printing technologies, Stereolithography (SLA) stands out as the most popular photopolymer resin-based technique offering the best resolution, precision, fine details and flawlessly smooth surface finishes[30,31]. SOLIDWORKS software is used to create the CAD designs for the samples and these drawings are then converted to STL files. After that, the STL files are loaded into the CHITUBOX program for slicing of the CAD model, where several printing parameters are set, including layer height, bottom exposure time, single

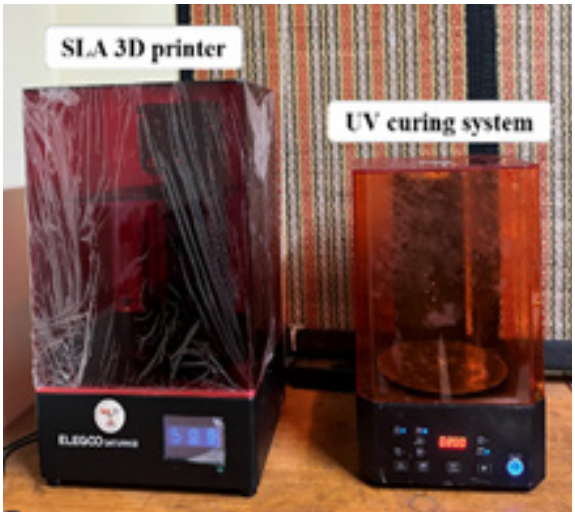


Figure 5. SLA 3D printer and UV curing system.

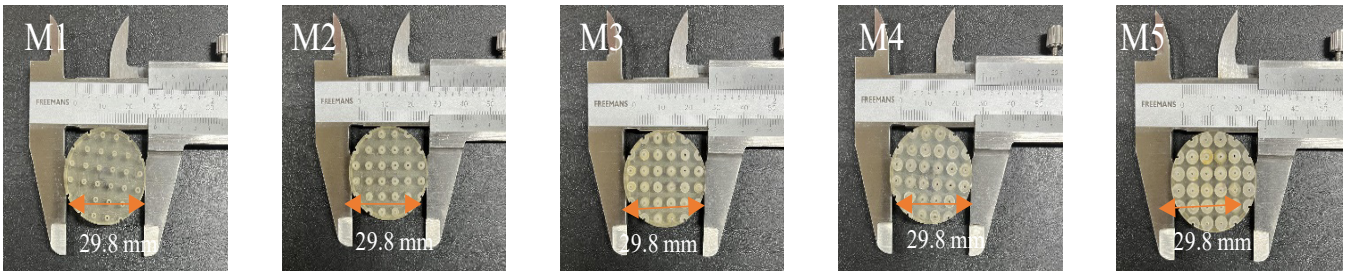


Figure 6. Diameter of samples M1, M2, M3, M4 and M5.

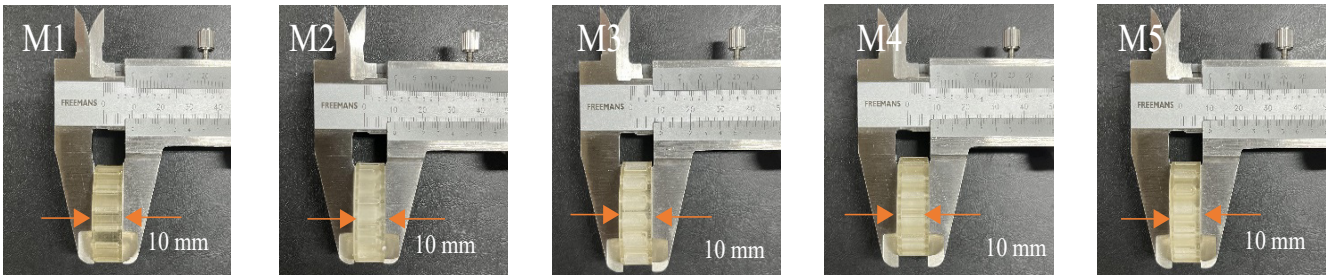


Figure 7. Thickness of samples M1, M2, M3, M4 and M5.

layer exposure duration, support type selection (heavy, medium or light), support density and infill density. After the CAD models are sliced, the files are transferred to the 3D printer (model: ELEGOO Saturn S) for printing.

After the printing is complete, the samples are cleaned with isopropyl alcohol to eliminate any remaining photopolymer resin from their surfaces and inside structural components. Then, using a cutter, the supports are taken out. To eliminate any last bits of resin from the interior structure, foreign items and leftover resin are removed using a compressed air jet. To achieve their greatest strength, the samples are finally subjected to Ultraviolet (UV) curing. The purpose of this rigorous process is to ensure that usable, high-quality samples are produced. Figure 5 shows the 3D printer that is used for the sample creation. Five samples are created each measuring 29.8mm ϕ and 10mm thickness (Figures 6 and 7).

2.5 Experiment for Acoustic Insulation Characteristics

The acoustic insulation characteristics of all five samples (M1-M5) are measured in terms of STL. The STL for samples is measured by four microphones method in ITA following ASTM E2611:2019[32]. Figure 8 shows the laboratory setup for the measurement of STL and describes how the four microphones are positioned about the sample. Between the tube's upstream and downstream parts, the samples are firmly placed. The extreme left of the tube has a loudspeaker mounted on it that produces white noise, which creates a plane wave condition inside the tube. An anechoic with a rigid termination is found on the other side of the tube. The incident acoustic pressure is recorded by microphones in the upstream part and the transmitted pressure is measured in the downstream part. Equations (1)-(4) are thus used to calculate the acoustic pressure at each microphone with x_1, x_2, x_3, and x_4 representing the distances between the sample and the corresponding microphones (m_1, m_2, m_3 and m_4). The transmitted and reflected sound in the second chamber is represented by C and D in these equations, whereas the incident and reflected sound in the first chamber is represented by A and B (see Equations (5)-(8)).

$$P_1 = \left(Ae^{-jkx_1} + Be^{jkx_1}\right)e^{j\omega t} \quad (1)$$

$$P_2 = \left(Ae^{jkx_2} + Be^{-jkx_2}\right)e^{j\omega t} \quad (2)$$

$$P_3 = \left(Ae^{-jkx_3} + Be^{jkx_3}\right)e^{j\omega t} \quad (3)$$

$$P_4 = \left(Ae^{jkx_4} + Be^{-jkx_4}\right)e^{j\omega t} \quad (4)$$

$$A = j\frac{P_1e^{-jkx_2} - P_2e^{-jkx_1}}{2sink(x_1 - x_2)} \quad (5)$$

$$B = j\frac{P_2e^{jkx_1} - P_1e^{jkx_2}}{2sink(x_1 - x_2)} \quad (6)$$

$$C = j\frac{P_3e^{jkx_4} - P_4e^{jkx_3}}{2sink(x_4 - x_3)} \quad (7)$$

$$D = j\frac{P_4e^{-jkx_3} - P_3e^{-jkx_4}}{2sink(x_4 - x_3)} \quad (8)$$

Two set-ups of the sound downstream, with the closed field (subscript 1) and open field (subscript 2) are used to collect the data. These set-ups are then assembled using Equation (9) to solve for α.

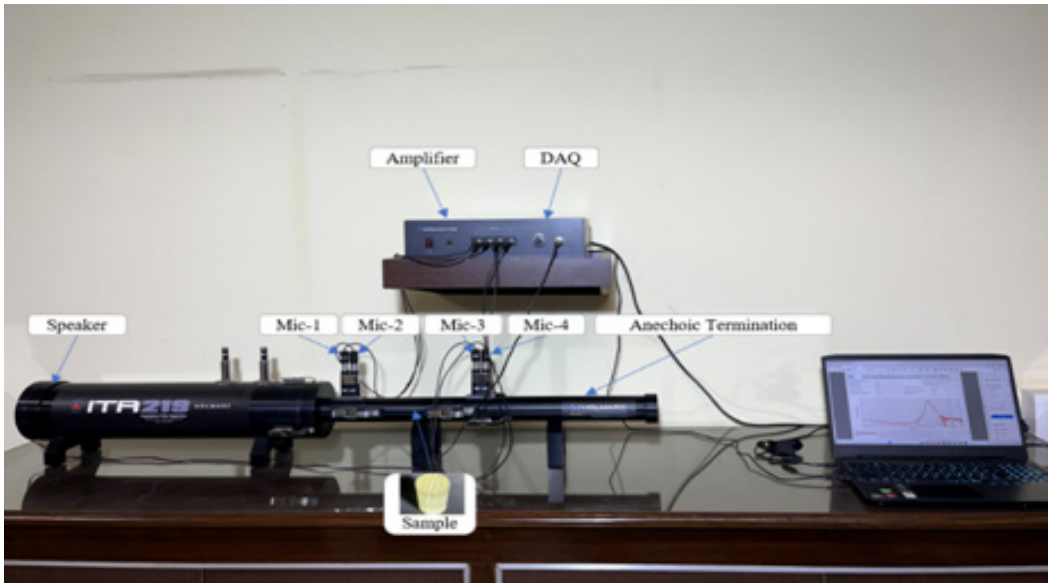


Figure 8. Impedance tube apparatus set-up for measurement of STL.

$$\alpha = \frac{A_1 D_2 - A_2 D_1}{C_1 D_2 - C_2 D_1} \tag{9}$$

The acoustic pressure levels observed in the two chambers are represented by the variables A_1, C_1, D_1 and A_2, C_2 and D_2 in this equation. Thus, the components of forward and backward acoustic waves are combined in the STL matrix, as shown in Equation (10).

$$\begin{Bmatrix} A \\ B \end{Bmatrix} = \begin{bmatrix} \alpha & \beta \\ \gamma & \delta \end{bmatrix} \tag{10}$$

Here, α and δ stand for the test sample's pressure transmission loss coefficients, which are found in the first and receiving chambers, respectively. The waveguide's acoustic impedance parameters are denoted by β and γ. Following this, Equation (11) can be used to calculate the STL.

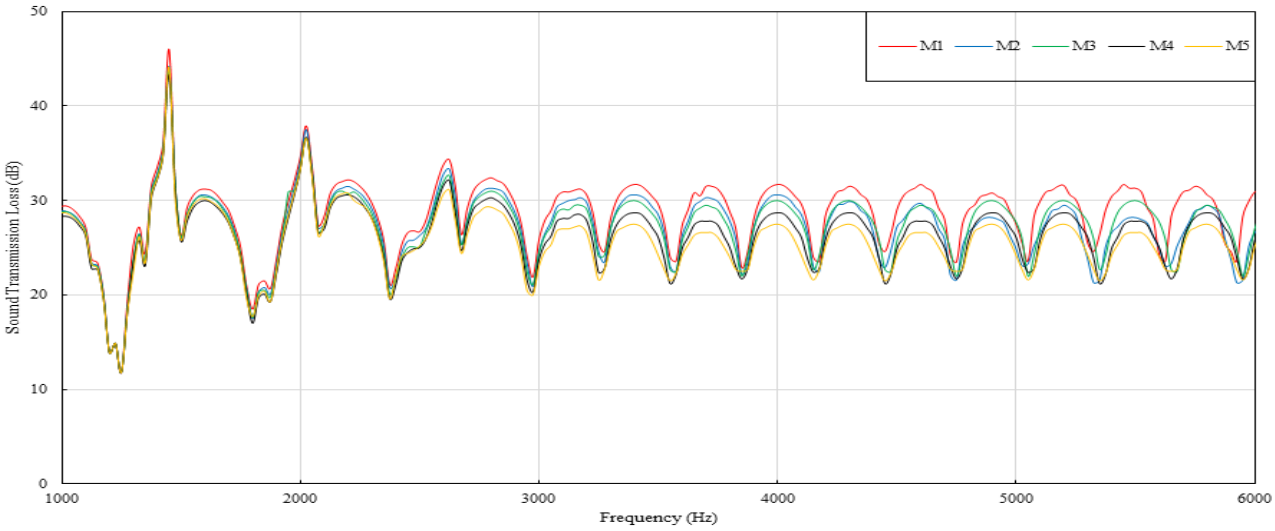


Figure 9. Frequency vs. STL plot for samples M1 to M5.

$$STL = -20\log(\alpha) \quad (11)$$

3.0 Results and Discussion

3.1 Experimental Consistency

Numerous elements, including ambient circumstances, instrument calibration and random fluctuations, might impact the measurement of acoustic qualities. The measurements are made four times for each sample to guarantee uniformity and consistency in the results. There is no difference in the results observed for any sample.

3.2 Sound Transmission Loss (STL)

STL measured in ITA for all samples from M1-M5 are graphically presented in Figure 9. Interestingly, there is a periodic trend in the STL variation across frequencies for all five samples. Sample M1, the least area expansion ratio (m) of 4 shows a higher STL of 46dB at 1.45kHz and a lower STL of 29.4dB at 1kHz. This fluctuation is also evident in sample M5, with a maximum STL of 44.1dB at 1.45kHz and a minimum STL of 26.6dB at 3.7kHz, 4.6kHz, and 5.5kHz.

The STL of all five samples expresses characteristics comparable to tunable acoustic material with an internal inline cavity structure[12] and classical SEC[9]. One interesting finding is that above 2.7kHz all five samples continue a periodic pattern and STL varies from 20dB to 32.4dB. This is because the STL curve's periodic pattern is created by the sudden change in characteristic impedance that follows the abrupt shift in cross-sectional area. Interestingly, the STL of all samples is above 20dB in the frequency (3-6 kHz) sensitive to NIHL.

3.2.1 Statistical Analysis of STL Results

The STL plots for samples M1-M5 are very close and difficult for comprehensive interpretation. Therefore statistical analysis is carried out using ANOVA (Analysis of Variance) to differentiate the mean of STL for the samples. A total of 233 STL values (sampled at 25 Hz intervals within the test frequency range) for each sample are used for ANOVA (Table 2). The null hypothesis (H_0) is that the individual datasets do not differ significantly from each other. Table 3 represents the results of the ANOVA test. The value of F > F critical means the test is significant. Also, $P \leq 0.05$ means H_0 is rejected and the alternate hypothesis (H_1) is true. The above results summarily indicate that the STL properties of the samples are not identical but it is difficult to conclude on the superiority of one or more samples over the others. Therefore visualisation of peak STL is required. It is further observed that the mean STL is highest over the test range for M1 (28.258dB).

Table 2. Summary of data set for ANOVA test

Groups		Count	Sum (dB)	Mean (dB)	SD
M1		233	6584.1	28.258	4.522
M2		233	6267.4	26.899	4.363
M3		233	6309.7	27.080	4.273
M4		233	6080.5	26.097	4.177
M5		233	5948.9	25.532	4.061

Table 3. Result of ANOVA test

Source of Variation	SS	df	MS	F	P-value	F critical
Between Groups	1005.045	4	251.261	13.703	6.37E-11	2.380

Table 4. Peak STLs and corresponding frequencies for samples M1 to M5

Peak TL Frequency (Hz)	Peak STL (dB)				
	M1	**M2**	**M3**	**M4**	**M5**
1450	46.0	44.2	43.7	43.3	44.1
1600	31.2	30.6	30.4	30.0	30.2
2025	37.9	37.5	36.6	36.7	36.6
2200	32.2	31.5	30.7	30.6	30.8
2625	34.3	33.3	32.6	32.1	31.1
2800	32.4	31.3	31.0	30.3	29.3
3175	31.2	30.3	29.5	28.5	27.3
3400	31.7	30.6	30.0	28.7	27.5
3700	31.5	30.3	29.5	27.8	26.6
4000	31.7	30.6	30.0	28.7	27.5
4300	31.5	29.9	30.0	28.7	27.5
4600	31.7	29.7	29.5	27.8	26.6
4900	30.8	28.2	30.0	28.7	27.5
5200	31.6	29.5	30.0	28.7	27.5
5500	31.3	28.2	30.0	27.8	26.6
5800	30.6	29.5	29.5	28.7	27.5

3.2.2 Influence of the Area Expansion Ratio on STL

Our findings show that samples of lesser area expansion ratio (m) (samples M1) produce higher STL, representing better acoustic insulation qualities. The frequencies corresponding to peak STL for all the samples are the same i.e. at 1.45kHz. Additionally, it is found that samples of lesser m showed marginally better performances in terms of STL as the acoustic wave passing through such sample drops more energy (via viscous and thermal losses) than the acoustic wave passing through the samples with higher m. With the peak STL values varying from 44.1- 46dB at 1.45kHz, all five samples stand out, indicating that their improved performance is a result of special structural features. To lower noise pollution and thereby improve acoustic comfort in real-world situations, these findings offer *insightful* information for the creation of cutting-edge acoustic materials for soundproofing and noise control applications. Table 4 displays the peak STLs and corresponding peak Transmission Loss (TL) frequencies for five samples.

Overall, the potential of SEC structure in the design and construction of AMM is demonstrated in the study. The sound insulation characteristic is thoroughly assessed in this work over a wide frequency range of 1-6kHz although our specific target range is 3-6kHz. The AMM having only 10mm thickness and made out of an additive manufacturing process demonstrates an amazing ability to attenuate at least 21.5dB in our targeted frequency range of 3-6kHz, which is impossible with conventional material.

It makes sense to believe that acoustic property like STL is significantly influenced by the area expansion ratio. In the present research, only the STL of the designed samples are measured and analysed. In the future other acoustic characteristics like sound absorption can be

studied for these samples. The printing accuracy of the available SLA 3D printer restricts manufacturing freedom, which is based on the periodic reproduction of unit cells and prevents the diameter of both inlet and outlet ports from being less than 1mm. Future research with higher-resolution 3D printers will allow for the investigation of the acoustic characteristics of different structures and complicated designs.

4.0 Conclusion

Several key factors like how physical dimensions and SEC structure collectively enhance the acoustic performance of photopolymer resin materials are discussed. Based on sample design, testing of samples and redesign of samples, novel AMMs with configurable acoustic properties are created. The focus of the present research is to develop an AMM for the design of control rooms in ore handling and mineral beneficiation plants. Promising outcomes are observed for STL as enumerated below.

- The STL values are varied with the more or less similar periodic pattern even if the area expansion ratio (m) changes.
- The AMMs designed and developed in this work have the potential to attenuate at least 21.5dB in the 3-6kHz targeted frequency band, which satisfies our criteria of attenuating at least 15dB for practical use.
- AMM having a lesser area expansion ratio of SEC exhibits greater acoustic insulation characteristics.
- Further research is required for a fuller understanding of the physics behind the periodic nature of the STL to develop specialised acoustic solutions for the design of control rooms.

Suitable acoustic metamaterials like those with adjustable acoustic qualities must be selected on priority when designing and constructing control rooms with specific sound reduction characteristics within a target frequency range. Overall, this study establishes the foundation for the creation of AMM based on SEC structure. The material shows great promise for use in acoustic insulation applications in control rooms to protect the operators from hazardous noise exposure in factories and plants.

5.0 Statement of Data Availability

The datasets produced and/or examined in this study can be obtained from the corresponding author upon reasonable request.

6.0 Statement of Author Contribution

Nihar Ranjan Sahu: Conceptualisation, data curation, formal analysis, investigation, methodology, software, visualisation, writing the original draft, writing the review and editing.

Bibhuti Bhusan Mandal: Supervision, conceptualization, writing, review and editing.

7.0 Acknowledgements

The authors gratefully acknowledge the Department of Mining Engineering at the Indian Institute of Technology Kharagpur for providing the laboratory facilities in the Noise Lab for conducting experiments and fabricating materials.

8.0 Funding

This research was not supported by any specific grant from funding agencies in the commercial, public or non-profit sectors.

9.0 References

1. Nelson DI, Nelson RY, Concha-Barrientos M, Fingerhut M. The global burden of occupational noise-induced hearing loss. American J Industrial Med. 2005; 48:446-58. https://doi.org/10.1002/ajim.20223 PMid:16299704.
2. Nandi S, Dhatrak S. Occupational noise-induced hearing loss in India. Indian J Occup Environ Med. 2008; 12:53. https://doi.org/10.4103/0019-5278.43260 PMid:20040978 PMCid: PMC2796754.
3. British Society of Audiology. Pure-tone air-conduction and bone-conduction threshold audiometry with and without masking; 2018.
4. Boger ME, Barbosa-Branco A, Ottoni, ÁC. The noise spectrum influences on noise-induced hearing loss prevalence in workers. Braz J Otorhinolaryngol.

2009; 75:328-34. https://doi.org/10.1590/S1808-86942009000300003PMid:19649479.
5. Manwar V, Mandal B, Pal A. Environmental propagation of noise in mines and nearby villages: A study through noise mapping. Noise Health. 2016; 18:185. https://doi.org/10.4103/1463-1741.189246 PMid:27569406 PMCid:PMC5187660.
6. NIOSH. Noise Control Resource Guide - Surface Mining; 1999.
7. Gelfand & Stanley. Essentials of audiology. Thieme; 2011.
8. Directorate General of Mines Safety. DGMS (Tech) Circular No. 18 of 1975: Protection of workers against noise and vibration in the working environment. Dhanbad, India.
9. Munjal ML. Noise and vibration control. Sci World. 2013. https://doi.org/10.1142/8614 PMid:25737873.
10. Munjal ML. Acoustics of ducts and mufflers. Wiley; 2014.
11. Sahu, NR, Mandal BB. Investigating the acoustic performance of metamaterials with internal simple expansion chamber structure. In INTER-NOISE and NOISE-CON Congress and Conference Proceedings Institute of Noise Control Engineering. 2024; 270(3):8180-8190. https://doi.org/10.3397/IN_2024_4056
12. Sahu NR, Mandal BB. Developing tunable acoustic materials with inline cavity structure for enhanced sound absorption and transmission loss. J Build Eng. 2024; 82:108305. https://doi.org/10.1016/j.jobe.2023.108305.
13. WOL 3D Technical specification of standard UV-cured resin. Availble from: https://worldoflilliputs.com/product/itech-lcd-standard-resin-grey-500ml/
14. Chen Z, Chong Lim KM, Lee HP. Reconfigurable 3D printed acoustic metamaterial chamber for sound insulation. Int J Mech Sci. 2024; 266:108978. https://doi.org/10.1016/j.ijmecsci.2024.108978.
15. Sahu NR, Mandal BB. Development of acoustic material with inline cavity structure for design of operators' cabins in mineral processing plants. In INTER-NOISE and NOISE-CON Congress and Conference Proceedings Institute of Noise Control Engineering. 2023; 268(3)5688-5699. https://doi.org/10.3397/IN_2023_0810
16. Katiyar N, Choudhury SS, Kant R, Bhattacharya S. Low-frequency noise attenuation through hybrid perforated hemispherical shells and membrane-type acoustic metamaterial. J Appl Phys. 2024; 136(1):013104. https://doi.org/10.1063/5.0200573.
17. Katiyar N, Choudhury Ss, Saha R, Bhattacharya S. Broadband low-frequency noise attenuation with parallel U-shaped membrane resonators. In INTER-NOISE and NOISE-CON Congress and Conference Proceedings. Institute of Noise Control Engineering. 2024; 270(11):83-94. https://doi.org/10.3397/IN_2024_1625
18. Berger JB, Wadley HNG, McMeeking RM. Mechanical metamaterials at the theoretical limit of isotropic elastic stiffness. Nature. 2017; 543:533-37. https://doi.org/10.1038/nature21075 PMid:28219078.
19. Deshpande VS, Fleck NA, Ashby MF. Effective properties of the octet-truss lattice material. J Mech Phys Solids. 2001; 49:1747-69. https://doi.org/10.1016/S0022-5096(01)00010-2
20. Dong L, Deshpande V, Wadley H. Mechanical response of Ti-6Al-4V octet-truss lattice structures. Int J Solids Struct. 2015; 60-61:107-124. https://doi.org/10.1016/j.ijsolstr.2015.02.020
21. Zheng, X. et al. Ultralight, ultrastiff mechanical metamaterials. Science. 2014; 344:1373-7. 2014. https://doi.org/10.1126/science.1252291.
22. Egan PF, Gonella VC, Engensperger M, Ferguson SJ, Shea K. Computationally designed lattices with tuned properties for tissue engineering using 3D printing. PLoS ONE. 2017; 12:e0182902. https://doi.org/10.1371/journal.pone.0182902 PMid:28797066 PMCid:PMC5552288.
23. Meza LR. et al. Reexamining the mechanical property space of three-dimensional lattice architectures. Acta Materialia. 2017; 140:424-32. https://doi.org/10.1016/j.actamat.2017.08.052.
24. Ashby MF. The properties of foams and lattices. Phil Trans R Soc A. 2006; 364:15-30. https://doi.org/10.1098/rsta.2005.1678 PMid:18272451.
25. Gibson LJ. Cellular solids. MRS Bull. 2003; 28:270-4. https://doi.org/10.1557/mrs2003.79.
26. Warren WE, Kraynik AM. Linear elastic behavior of a low-density Kelvin foam with open cells. Int J Appl Mech. 1997; 64:787-94. https://doi.org/10.1115/1.2788983.
27. Sahu NR, Mandal BB. Design of operators' cabins for mineral processing plants using specially fabricated acoustic material with simple expansion chamber structure. In Proceedings of the 10th Asian Mining Congress. Sinha A, Sarkar BC. and Mandal PK, editors.

Switzerland, Cham: Springer Nature; 2023. p. 376-386 https://doi.org/10.1007/978-3-031-46966-4_31 PMCid: PMC10568053.

28. Sahu NR, Mandal BB. Impact of air gap thickness on acoustic metamaterials with internal simple expansion chamber structure. In INTER-NOISE and NOISE-CON Congress and Conference Proceedings Institute of Noise Control Engineering. 2024; 270(3):8030-8041. https://doi.org/10.3397/IN_2024_4039.
29. Holmarc Opto-Mechatronics Ltd. Impedance Tube Apparatus (HO-AE-ITA219) user manual. Availble from: https://www.holmarc.com/pdf/impedence_tube.pdf
30. Sai Saran O, Reddy AP, Chaturya L, Pavan Kumar M. 3D printing of composite materials: A short review. Mater Today: Proceedings. 2022; 64:615-9. https://doi.org/10.1016/j.matpr.2022.05.144.
31. Fusaro G, Barbaresi L, Cingolani M, Garai M, Ida E, Prato A, Schiavi A. Investigation of the impact of additive manufacturing techniques on the acoustic performance of a coiled-up resonator. J Acoust Soc Am. 2023; 153(5):2921-2921. https://doi.org/10.1121/10.0019474.
32. ASTM E2611. Standard test method for normal incidence determination of porous material acoustical properties based on the transfer matrix method; 2019